Application of the diffusion kurtosis model for the study of breast lesions

Luísa Nogueira · Sofia Brandão · Eduarda Matos · Rita Gouveia Nunes · Joana Loureiro · Isabel Ramos · Hugo Alexandre Ferreira

L. Nogueira (✉)
Department of Radiology, School of Health Technology of Porto/ Polytechnic Institute of Porto (ESTSP/IPP), Rua Valente Perfeito, 322, 4400-330 Vila Nova de Gaia, Portugal
e-mail: mlpnogueira@med.up.pt

L. Nogueira
e-mail: mlpnogueira@gmail.com

S. Brandão · J. Loureiro
MRI Unit, Department of Radiology, Hospital de São João, Alameda Prof. Hernâni Monteiro, 4200-319 Porto, Portugal

S. Brandão
e-mail: sofia.brand@gmail.com

J. Loureiro
e-mail: joanaploureiro@gmail.com

E. Matos
Department of Health Community, Institute of Biomedical Sciences Abel Salazar (ICBAS), University of Porto, Rua de Jorge Viterbo Ferreira, 228, 4050-313 Porto, Portugal
e-mail: ematos@icbas.up.pt

R. G. Nunes · H. A. Ferreira
Institute of Biophysics and Biomedical Engineering (IBEB), Faculty of Sciences, University of Lisbon, Campo Grande, 1749-016 Lisboa, Portugal

R. G. Nunes
e-mail: rgnunes@fc.ul.pt

H. A. Ferreira
e-mail: hhferreira@fc.ul.pt

I. Ramos
Head Department of Radiology, Hospital de São João/Faculty of Medicine of Porto University (FMUP), Alameda Prof. Hernâni Monteiro, 4200-319 Porto, Portugal
e-mail: radiologia.hsj@mail.telepac.pt

Abstract

Objectives To evaluate diffusion-weighted imaging (DWI) and diffusion kurtosis imaging (DKI) in the differentiation and characterisation of breast lesions.

Methods Thirty-six women underwent breast magnetic resonance imaging (MRI) including a DWI sequence with multiple b-values (50–3,000 s/mm^2). Mean values for apparent diffusion coefficient (ADC), mean diffusivity (MD) and mean kurtosis (MK) were calculated by lesion type and histological subtype. Differences and correlation between parameters were determined.

Results Forty-four lesions were found. There were significant differences between benign and malignant lesions for all parameters (ADC, $p=0.017$; MD, $p=0.028$; MK, $p=0.017$). ADC and MD were higher for benign ($1.96\pm0.41\times10^{-3}$ and $2.17\pm0.42\times10^{-3}$ mm^2/s, respectively) than for malignant lesions ($1.33\pm0.18\times10^{-3}$ and $1.52\pm0.50\times10^{-3}$ mm^2/s). MK was higher for malignant (0.61 ± 0.27) than benign lesions (0.37 ± 0.18). We found differences between invasive ductal carcinoma (IDC) and fibroadenoma (FA) for all parameters (ADC, MD and MK): $p=0.016$, 0.022 and 0.016, respectively. FA and fibrocystic change (FC) showed differences only in MK ($p=0.016$).

Conclusions Diffusion in breast lesions follows a non-Gaussian distribution. MK enables differentiation and characterisation of breast lesions, providing new insights into microstructural complexity. To confirm these results, further investigation in a broader sample should be performed.

Key Points

- *The diffusion kurtosis model provides new information regarding breast lesions*
- *MD and MK are valid parameters to characterise tissue microstructure*
- *MK enables improved lesion differentiation*
- *MK is able to differentiate lesions that display similar ADC values*

Keywords Diffusion weighted imaging · Diffusion kurtosis imaging · Magnetic resonance imaging · Breast lesions · Mean kurtosis

Abbreviations

DWI	Diffusion-weighted imaging
ADC	Apparent diffusion coefficient
PDF	Probability of displacement function
DKI	Diffusion kurtosis imaging
MD	Mean diffusivity
MK	Mean kurtosis
IDC	Invasive ductal carcinoma
ILC	Invasive lobular carcinoma

Introduction

Diffusion-weighted imaging (DWI) in breast imaging is a widespread tool used in the differential diagnosis of breast lesions [1–6]. When applying DWI to breast lesions, a mono-exponential model is used to fit signal intensity (SI) decay between two or more b-values and quantify the apparent diffusion coefficient (ADC):

$$ln[S(b)] = ln[S(0)] - bADC \quad (1)$$

where *S(b)* and *S(0)* are the signal intensity at the echo time for different b-values and *b* the diffusion sensitising value. This model is based on the assumption that the microenvironment is homogeneous, and also that the probability displacement function (PDF) describing the displacement of water molecules associated with diffusion follows a Gaussian distribution [7]. However, biological tissues present natural barriers (such as cell membranes) and cellular compartments (such as organelles) that constrain water motion [8], resulting in a PDF with a more peaked profile when compared with that of a Gaussian distribution. The kurtosis excess is an index which reflects the peak of a distribution and can be used to quantify how much the PDF deviates from the Gaussian shape. This deviation reflects tissue microstructure complexity [9], with the kurtosis parameters serving as an index for lesion characterisation.

A preliminary study developed by our group focused on the usefulness of performing visual lesion assessment using large b-values (2,000 and 3,000) s/mm^2 has confirmed that SI attenuation when using higher b-values was no longer described by a mono-exponential fitting. Nonetheless, in the clinical setting, only the mono-exponential fitting is used on MR, which conditions ADC quantification when higher b-values are used [10].

Jensen et al. [9] first introduced the diffusion kurtosis imaging (DKI) model. DKI is an extension of conventional DWI, which accounts for non-Gaussian PDF distribution, therefore further reflecting tissue complexity [9]. DKI requires the use of high b-values to observe the non-Gaussian behaviour of water diffusion [11].

To obtain the kurtosis diffusional parameters, a fit is performed with the signal decay modelled by the equation [9]:

$$ln[S(b)] = ln[S(0)] - bMD + \frac{1}{6}b^2MD^2\ MK + O(b^3) \quad (2)$$

where MD is the mean diffusivity, MK is the mean kurtosis and $O(b^3)$ is the fit error associated to the measurement. Both parameter estimates reflect diffusion along the direction of the diffusion sensitising gradients.

The MK parameter is a dimensionless metric. Comparing Eqs. 1 and 2, it becomes clear that when MK is equal to zero, MD becomes equal to ADC, and the PDF follows a Gaussian distribution. A positive MK corresponds to a more peaked PDF, which explains why lesions with a more complex microstructure display higher MK values [12].

Studies concerning DKI were developed in animal models, brain, lungs, prostate and squamous cell carcinoma [13–18] but, to the best of our knowledge, there is a lack of published studies regarding the application of DKI in breast [19]. Adding MK may potentially result in higher sensitivity to pathological tissue changes. Thus, our goal was to assess the role of DWI and DKI models to differentiate and characterise breast lesions.

Materials and methods

Subjects

This prospective study was included in a wider investigation, and received approval from the Institutional Review Board (CES 276/13). Written informed consent was obtained from all patients.

Clinical indication for breast magnetic resonance imaging (MRI) included women with: BRCA mutation (5), suspicious lesions (17), identification of occult carcinoma (4), detection of residual carcinoma (2), pre-operative evaluation (10), post-surgery follow-up (3) and evaluation of breast implants (2).

Exclusion criteria to DWI were applied to women who: had been submitted to breast surgery, radiotherapy and/or chemotherapy within the previous 48 months (5); had cystic lesions and/or breast implants (2); presented an undetectable

enhancing lesion on dynamic contrast-enhanced (DCE) images. The final sample included 36 women.

Acquisition protocol

MRI examinations were performed using a 3-T system (Tim Trio; Siemens, Erlangen, Germany) and a four-channel bilateral breast coil. Patients were positioned in the prone position.

The acquisition protocol included morphological sequences: axial bilateral T2-weighted (T2w) fast spin echo (FSE), sagittal unilateral T1w three-dimensional (3D) gradient echo (GRE) fast low angle shot (FLASH) and sagittal unilateral T2w FSE with short tau inversion recovery (STIR). A conventional DWI unilateral sagittal single-shot spin-echo echo planar imaging (SS-SE-EPI) sequence with eight b-values was performed before gadolinium injection, with gradients sensitisation applied in the *x*, *y* and *z* directions to generate three-scan-trace images. This sequence included a larger number and higher b-values than typically used in the clinical practice. The inclusion of the b-values 2,000 and 3,000 s/mm^2 resulted in a TE of 106 ms. Finally, DCE axial images were acquired during six phases with gadolinium injection followed by unilateral sagittal fat-suppressed (water exCitation) T1w 3D FLASH images. Protocol details are shown in Table 1.

Image analysis

The imaging device workstation (Siemens Medical Systems, with a work in progress version 17A) was used for image analysis. Firstly, a radiologist (J.L.) with 6 years experience in breast-imaging reported the conventional MRI images using the Breast Imaging Reporting and Data System (BI-RADS)-MRI lexicon [20] for lesion classification.

DWI datasets were analysed in consensus by two radiology researchers. Each lesion was observed in the DW images based on the MRI report, and using the T2w, DCE and the post-contrast images, serving as a roadmap for regions of interest (ROIs) demarcation. Firstly, ROIs demarcation were performed for each lesion at b=400 s/mm^2, and then copied to the other b-values. This b-value was chosen due to the high contrast between the lesion core and its outer limits. For each lesion, a fixed size ROI (0.25 cm^2) was drawn to include the area of highest SI. The mean value and standard deviation (SD) of the SI were recorded.

These SI values were fitted with two different models: a mono-exponential function for the range b=50−1,000 s/mm^2 (Eq. 1) and a DKI model using the higher b-values ranging from 50 to 3,000 s/mm^2 (Eq. 2) additionally. For this purpose, an in-house script was developed in MATLAB software (Mathworks, Cambridge, UK.) using the Levenberg-Marquardt algorithm [19, 21]. The ADC, MD and MK were then estimated for each lesion.

Statistical analysis

Mean values for each parameter were calculated for all lesions, by lesion type and histological subtype. Differences in mean values were tested using the Mann-Whitney test. Correlation between parameters was analysed by Spearman coefficient (r_S). PASW Statistics V17 software was used. Statistical significance was set at $p<0.05$.

Table 1 Scan protocol for conventional MRI and DWI pulse sequence

Parameters	Conventional pre-contrast			DWI-SPAIR	Dynamic	Post contrast
Sequence	T2w TSE	T1w 3D Flash	T2w TSE	Single-shot EPI	T1w 3D Flash	T1w 3D Flash
Orientation	Axial Bilateral	Sagittal	Sagittal	Sagittal	Axial Bilateral	Sagittal
TR/TE (ms)	4990/88	17/4.9	4920/67	4900/106	3.77/1.42	7.8/3.9
TI (ms)	_	_	210	_	_	_
Fat suppression	_	_	STIR	SPAIR	SPAIR	Water excitation
FOV (mm^2)	320×320	200×200	200×200	250×250	320×320	160×160
Matrix	512×384	275×384	448×314	84×128	358×448	256×256
Slice thickness	4	2	4	5	0.9	0.9
Number of slices	26	64	26	16	160	144
NEX	2	1	2	3	1	1
Bandwidth (Hz/pixel)	305	430	248	1628	490	450
Scan time (min)	2:06	3:49	4:26	5:58	4:32	3:12
b-values (s/mm^2)	_	_	_	50, 200, 400, 600, 800, 1000, 2000 and 3000	_	_

DWI-SPAIR diffusion-weighted imaging with spectrally adiabatic inversion recovery, *TSE* turbo spin echo, *T1w 3D Flash* three-dimensional gradient echo fast low angle shot, *EPI* echo planar imaging, *TR/TE* repetition time/echo time, *TI* inversion time, *STIR* short tau inversion recovery, *FOV* field of view, *NEX* number of excitations

Results

Patients and lesions characteristics

The final sample included 36 women with 44 lesions detected in both the DCE and DWI. Histopathological proof was obtained for 40 lesions. Malignant lesions were: ductal carcinoma in situ (DCIS) (2); invasive ductal carcinoma (IDC) (19); lobular carcinoma in situ (LCIS) (1); invasive lobular carcinoma (ILC) (9). Among benign lesions there were: fibroadenomas (FAs) (7), epithelial proliferative lesion (EPL) (1), fibrocystic change (FC) (1). Four additional lesions (1 FA and 3 FCs) were assumed as benign, based on morphological features and dimensional stability as observed by a 2-year follow-up.

Figure 1 displays MR images of a 39-year-old woman with a grade III invasive ductal carcinoma.

DWI and DKI: analysis of benign and malignant lesions

Table 2 presents mean values, derived from the mono-exponential (ADC) and kurtosis models (MD and MK), by lesion type.

There were significant differences for each of the parameters between lesion types. Mean ADC and MD values were higher in benign than in malignant lesions. Conversely, MK was higher for malignant lesions than for benign ones.

Figure 2 represents the distribution of ADC (Fig. 2a), MD (Fig. 2b) and MK (Fig. 2c) by lesion type, using the two models.

Application of mono-exponential and kurtosis models, by histological type

A descriptive analysis was performed for each model by histological type (Table 3).

Table 2 Descriptive analysis of ADC, MD and MK using the two models of DWI (mono-exponential and diffusion kurtosis), and differences by lesion type

Mean	Benign (n=13)	Malignant (n=31)	p*
ADC [a]	1.96±0.41	1.33±0.43	0.017
MD [a]	2.17±0.42	1.52±0.50	0.028
MK [b]	0.37±0.18	0.61±0.27	0.017

ADC apparent diffusion coefficient, *MD* mean diffusivity, *MK* mean kurtosis

[a] ADC and MD ($\times 10^{-3}$ mm^2 /s)

[b] MK is a dimensionless metric

*Statistical differences

There were significant differences for ADC, MD and MK between: IDC and FA (p=0.016, p=0.022 and p=0.016); IDC and FC (p=0.003, p=0.004 and p=0.003), as well as between ILC and FC (p=0.006, p=0.011 and p=0.034). For FA and FC, only MK showed statistical difference (p=0.283, p=0.386; and p=0.016).

Correlation between kurtosis parameters

Significant correlation was found between MD and MK for: all the lesions r_S=−0.636 (p<0.001), benign r_S=−0.588 (p=0.034) and malignant lesions r_S=−0.546 (p<0.001).

Discussion

Breast pathological processes display large heterogeneity [22]. It is also well known that lesions are not homogeneous, even within the same histological type [23].

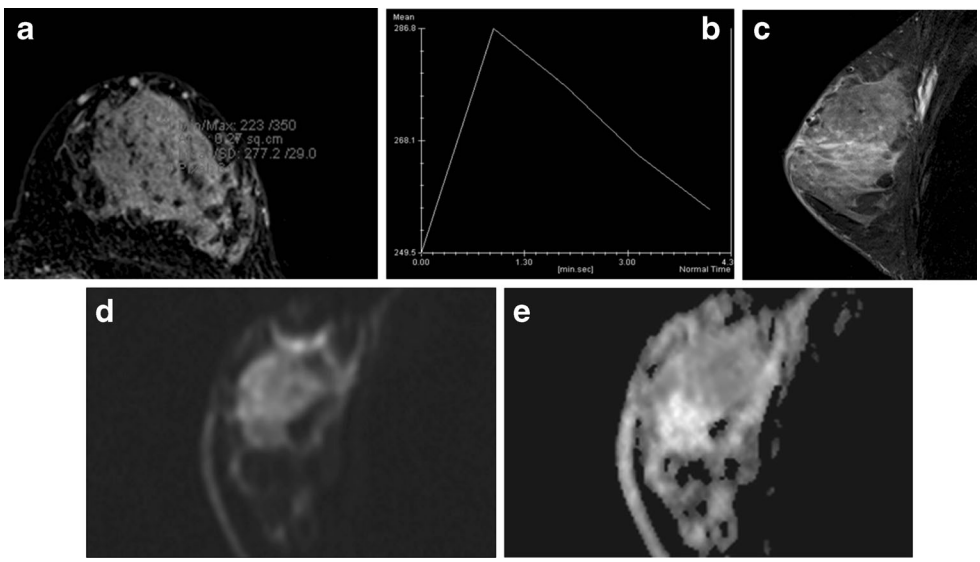

Fig. 1 A 39-year-old woman with suspicious malignant lesion in the upper left quadrant breast. **a** Dynamic contrast-enhanced acquisition image shows a mass with irregular borders and heterogeneous enhancement. **b** Signal intensity/time curve presents strong initially contrast enhancement followed by washout. **c** Sagittal post-contrast T1w 3D GRE FLASH. **d** DWI with a b-value of 1,000 s/mm^2 image shows a hyperintense lesion and **e** its respective mean ADC map, where the lesion is hypointense. Histological diagnosis: invasive ductal carcinoma, grade III

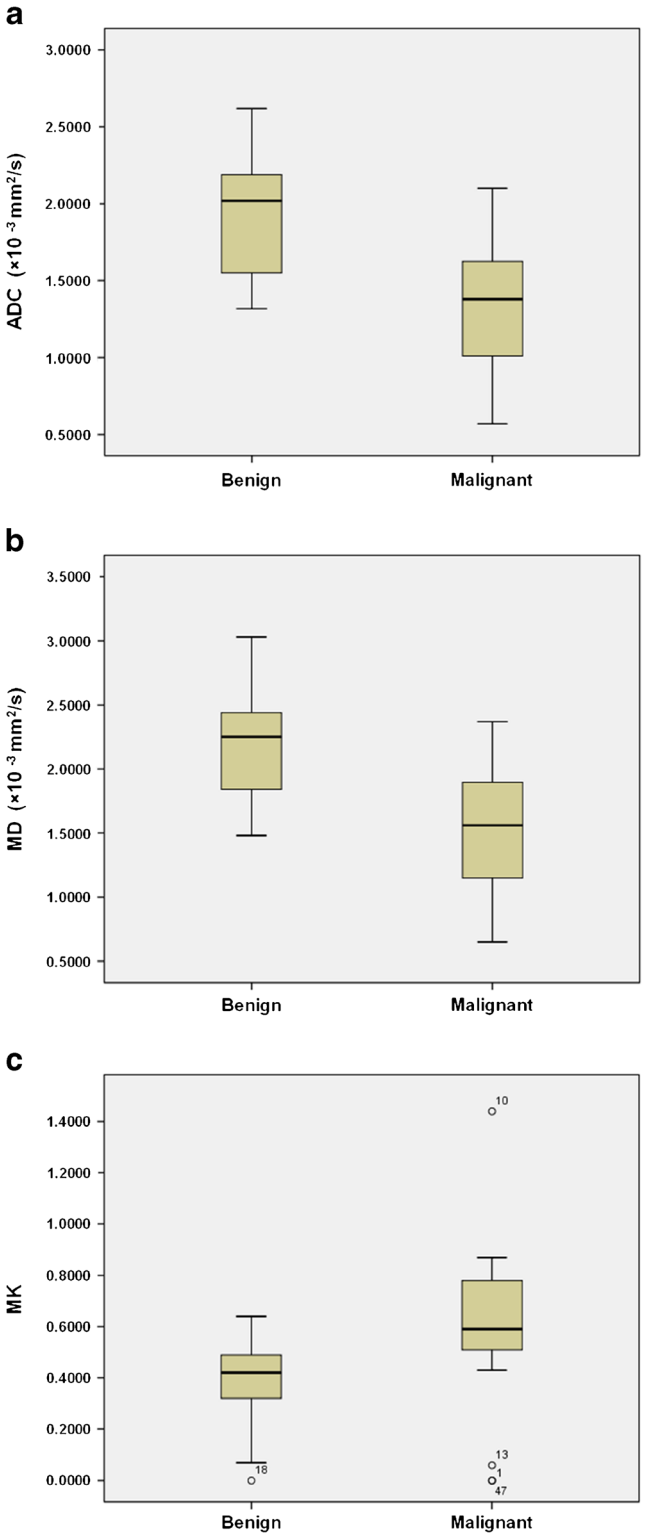

Fig. 2 Box plots distribution of the parameters by lesion type using the mono-exponential model ADC (**a**) and MD (**b**) and MK (**c**) using the kurtosis model. MK is a dimensionless metric

In standard DWI, it is assumed that water diffusion PDF follows a Gaussian distribution. However, complex microenvironment within tissues hampers water mobility and leads to a diffusion PDF that probably does not follow a Gaussian distribution [9]. Factors concurrent to the non-mono-exponential diffusion behaviour include macromolecular binding of water, restricted diffusion and water exchange between multiple compartments [24–26].

Table 3 Descriptive analysis for mono-exponential and kurtosis model by histological type

Histological type	Mono-exponential	Kurtosis	
	ADC ($\times10^{-3}$ mm^2/s)	MD ($\times10^{-3}$ mm^2/s)	MK [a]
DCIS (n=2)	1.31±0.43	1.50±0.50	0.33±0.47
IDC (n=19)	1.13±0.54	1.27±0.75	0.63±0.19
LCIS (n=1)	1.38	1.52	0.44
ILC (n=9)	1.43±0.45	1.62±0.51	0.63±0.38
FA (n=8)	1.82±0.44	2.08±0.52	0.48±0.09
EPL (n=1)	1.99	2.48	0
FC (n=4)	2.13±0.18	2.29±0.12	0.25±0.14

n number of lesions by histological type, *DCIS* ductal carcinoma in situ, *IDC* invasive ductal carcinoma, *LCIS* lobular carcinoma in situ, *ILC* invasive lobular carcinoma, *FA* fibroadenoma, *EPL* epithelial proliferative lesion, *FC* fibrocystic change

[a] MK is a dimensionless metric

In this study, significant differences between the ADC of benign and malignant lesions were found when the mono-exponential model was applied. Also, significant differences were found for MD and MK between lesion types. This feature means that MD and MK parameters could also be used as valid parameters in lesion differentiation.

We found MK values lower for benign than for malignant lesions, which means that the diffusion PDF of benign lesions was less deviated from a Gaussian distribution, corresponding to decreased restriction when compared to malignant lesions. These differences were expected, considering that solid benign lesions usually present lower microstructural complexity than malignant tumours [27]. Moreover, the fact that both benign and malignant lesions showed MK values greater than zero strongly suggests that water PDFs differ from a Gaussian distribution. This non-Gaussian behaviour is related to different cellular compartments and the presence of lipid macromolecules [28].

In cancerous tissues, the increased cellularity usually leads to more barriers within the tissues, which disturbs the regular balance between the extra-cellular and cellular fractions, leading to higher restriction to water diffusion [29]. Still, the movement of water molecules between compartments may be more or less restricted depending on membrane permeability [30]. A less cellular environment potentiates a larger extracellular space and facilitates water motion [31].

In our study, the EPL lesion showed MK close to zero, which suggests a decreased cellularity and a simple microstructure, closer to a homogeneous environment, without

impediment of water distribution between spaces. IDC and ILC evidenced high MK and low MD, which can be explained by their highly complex microstructures characteristic.

A study developed by Borlinhas et al. [19] presented significant differences between MD and MK for IDC and FA. They also observed that MD could distinguish IDC from DCIS. In our study, we found differences in MK between FA and FC, while ADC and MD could not differentiate them. This may have quite a high impact for non-invasive differential diagnosis, especially because FA and FC sometimes present overlapping ADCs within and with malignant lesions depending on fibrolastic/miofibrolastic components. However, given the low number of these type of lesions included in this study, the results should be considered carefully.

Additionally, we found that MD and MK are not perfectly monotonically related, i.e. MK contributes with additional information other than MD.

Our study presents some limitations. Firstly, the number of lesions is low for definitive conclusions. Secondly, the fact that ten (four benign and six malignant) lesions were biopsied before MRI could have influenced the measurements. Although we have always performed MRI after a minimum period of 8 days following biopsy, we cannot neglect that residual blood and/or oedema could influence the parameters. However, given the reduced number of cases, it was not possible to assess the effect of biopsy on tissue structure.

Another limitation was the imaging time. The use of the DKI model implies using higher b-values with increased TE, prolonging the examination time. Despite this inconvenience, our results suggested that MK could help distinguish different grades of celullarity within the same lesion group (FA vs FC). Given the wide spectrum of breast lesions, even within the same histology group, MK could play a role in such cases.

In conclusion, we have observed that ADC, MD and MK can differentiate benign from malignant breast lesions. Furthermore, our results suggest that the DKI model can help characterise the complex behaviour of water diffusion in breast lesions, particularly by discriminating microstructure differences within the same lesion type. At present, larger samples are being examined to clarify the role of DKI in breast imaging.

References

1. Guo Y, Cai YQ, Cai ZL, Gao YG, An NY, Ma L (2002) Differentiation of clinically benign and malignant breast lesions using diffusion-weighted imaging. J Magn Reson Imaging 16:172–178
2. Bogner W, Gruber S, Pinker K et al (2009) Diffusion-weighted MR for differentiation of breast lesions at 3.0 T: how does selection of diffusion protocols affect diagnosis? Radiology 253:341–351
3. Peters N, Vincken K, Van den Bosch M, Luijten P, Mali W, Bartels L (2010) Quantitative diffusion weighted imaging for differentiation of benign and malignant breast lesions: the influence of the choice of b-values. J Magn Reson Imaging 31:1100–1105
4. El Khouli R, Jacobs AM, Mezban DS, Huang P, Kamel JK, Bluemke AD (2010) Diffusion-weighted imaging improves the diagnostic accuracy of conventional 3.0-T breast MR imaging. Radiology 256: 64–73
5. Lo G, Ai V, Chan J et al (2009) Diffusion-weighted magnetic resonance imaging of breast lesions: first experiences at 3 T. J Comput Assist Tomogr 33:63–69
6. Pereira F, Martins G, Oliveira R (2011) Diffusion magnetic resonance imaging of the breast. Magn Reson Imaging Clin N Am 19:95–110
7. Basser PJ, Jones DK (2002) Diffusion-tensor MRI: theory, experimental design and data analysis—a technical review. NMR Biomed 15:456–67
8. Gillies R, Raghunand N, Karczmar G, Bhujwalla Z (2002) MRI of the tumor microenvironment. J Magn Reson Imaging 16:430–450
9. Jensen J, Helpern J, Ramani A, Lu H, Kaczynski K (2005) Diffusion kurtosis imaging: the quantification of non-Gaussian water diffusion by means of magnetic resonance imaging. Magn Reson Med 53: 1432–1440
10. Tamura T, Usui S, Murakami S et al (2012) Comparisons of multi b-value DWI signal analysis with pathological specimen of breast cancer. Magn Reson Med 68:890–897
11. Poot DH, Den Dekker AJ, Achten E, Verhoye M, Sijbers J (2010) Optimal experimental design for diffusion kurtosis imaging. IEEE Trans Med Imaging 29:3
12. Jansen J, Stambuk H, Koutcher J, Shukla-Dave A (2010) Non-Gaussian analysis of diffusion-weighted MR imaging in head and neck squamous cell carcinoma: a feasibility study. AJNR Am J Neuroradiol 31:741–748
13. Quentin M, Blondin D, Klasen J et al (2012) Comparison of different mathematical models of diffusion-weighted prostate MR imaging. Magn Reson Imaging 30:1468–1474
14. Cheung M, Hui E, Chan K, Helpen J, Qi L, Wu E (2009) Does diffusion kurtosis imaging lead to better neural tissue characterization? A rodent brain maturation study. Neuroimage 45:386–392
15. Falangola MF, Jensen JH, Babb JS et al (2008) Age-related non-Gaussian diffusion patterns in the prefrontal brain. J Magn Reson Imaging 28:1345–50
16. Chen S, Pickard JD, Harris NG (2003) Time course of cellular pathology after controlled cortical impact injury. Exp Neurol 1:87–102
17. Raab P, Hattingen E, Franz K, Zanella FE, Lanferman H (2010) Cerebral gliomas: diffusional kurtosis imaging analysis of microstructural differences. Radiology 254:876–81
18. Trampel R, Jensen JH, Lee RF, Kamenetskiy I, McGuinness G, Johnson G (2006) Diffusional kurtosis imaging in the lung using hyperpolarized 3He. Magn Reson Med 56:733–737
19. Borlinhas F, Lacerda L, Andrade A, Ferreira HA (2012) Diffusional kurtosis as a biomarker of breast tumors (E-poster presentation). European Congress of Radiology 2012, 1–5 March 2012, Vienna, Austria. doi:10.1594/erc2012/C-1369
20. Ikeda DM, Hylton NM, Kuhl CK et al (2003) BI-RADS: magnetic resonance imaging, 1st edn. In: D'Orsi CJ, Mendelson EB, Ikeda DM

et al (eds) Breast imaging reporting and data system: ACR BI-RADS—breast imaging atlas. American College of Radiology, Reston
21. Marquardt DW (1963) An algorithm for least-squares estimation of nonlinear parameters. J Soc Ind Appl Math 11:431–441
22. Costantini M, Belli P, Rinaldi P (2010) Diffusion-weighted imaging in breast cancer: relationship between apparent diffusion coefficient and tumour aggressiveness. Clin Radiol 65:1008–1012
23. Paran Y, Bendel P, Margalit R, Degani H (2004) Water diffusion in the different microenvironments of breast cancer. NMR Biomed 17: 170–180
24. Lyng H, Haraldseth O, Rofstad EK (2000) Measurement of cell density and necrotic fraction in human melanoma xenografts by diffusion weighted magnetic resonance imaging. Magn Reson Med 43:828–836
25. Sukstanskii AL, Yablonskiy DA (2002) Effects of restricted diffusion on MR signal formation. J Magn Reson 157:92–105
26. Kiselev VG, Il'yasov KA (2007) Is the "biexponential diffusion" biexponential? Magn Reson Med 57:464–469
27. Pereira F, Martins G, Oliveira R (2011) Diffusion magnetic resonance imaging of the breast. Magn Reson Imaging Clin N Am 19:95–110
28. De Santis S, Gabrielli A, Palombo M, Maraviglia B, Capuani S (2011) Non-Gaussian diffusion imaging: a brief practical review. Magn Reson Imaging 29:1410–1416
29. Fornasa F (2011) Diffusion-weighted magnetic resonance imaging: what makes water run fast or slow? J Clin Imaging Sci 1:1–7
30. Roth Y, Ocherashvilli A, Daniels D et al (2008) Quantification of water compartmentation in cell suspensions by diffusion-weighted and T2-weighted MRI. Magn Reson Imaging 26:88–102
31. Koh D, Collins D (2007) Diffusion-weighted MRI in the body: applications and challenges in oncology. AJR Am J Roentgenol 188:1622–1635